Direct Measurements of DT Fuel Preheat from Hot Electrons in Direct-Drive Inertial Confinement Fusion

A. R. Christopherson,[1,2] R. Betti,[1,2,3] C. J. Forrest,[1] J. Howard,[1,2] W. Theobald,[1] J. A. Delettrez,[1] M. J. Rosenberg,[1] A. A. Solodov,[1] C. Stoeckl,[1] D. Patel,[1,2] V. Gopalaswamy,[1,2] D. Cao,[1] J. L. Peebles,[1] D. H. Edgell,[1] W. Seka,[1] R. Epstein,[1] M. S. Wei,[1] M. Gatu Johnson,[4] R. Simpson,[4] S. P. Regan,[1] and E. M. Campbell[1]

[1]*Laboratory for Laser Energetics, University of Rochester, Rochester, New York 14623-1299, USA*
[2]*Department of Mechanical Engineering, University of Rochester, Rochester, New York 14623, USA*
[3]*Department of Physics and Astronomy, University of Rochester, Rochester, New York 14623, USA*
[4]*Plasma Science and Fusion Center, Massachusetts Institute of Technology, Cambridge, Massachusetts 02139, USA*

(Received 24 September 2020; revised 2 January 2021; accepted 11 June 2021; published 28 July 2021)

Hot electrons generated by laser-plasma instabilities degrade the performance of laser-fusion implosions by preheating the DT fuel and reducing core compression. The hot-electron energy deposition in the DT fuel has been directly measured for the first time by comparing the hard x-ray signals between DT-layered and mass-equivalent ablator-only implosions. The electron energy deposition profile in the fuel is inferred through dedicated experiments using Cu-doped payloads of varying thickness. The measured preheat energy accurately explains the areal-density degradation observed in many OMEGA implosions. This technique can be used to assess the viability of the direct-drive approach to laser fusion with respect to the scaling of hot-electron preheat with laser energy.

DOI: 10.1103/PhysRevLett.127.055001

In laser-driven inertial confinement fusion (ICF), a cryogenic shell of deuterium-tritium fuel is compressed inward by direct laser irradiation (direct drive) or by x rays from a laser-heated hohlraum (indirect drive) [1]. As the shell converges inward, it delivers PdV work to the central gaseous region, denoted as the hot spot. At stagnation, the final assembly consists of a low-density hot spot surrounded by a cold dense shell that provides the inertial confinement. For deuterium-tritium (DT) fuels, a minimum hot-spot areal density is required to slow down the alpha particles from the D + T fusion reactions driving the self-heating process. Furthermore, the areal density of the surrounding shell confines the hot-spot pressure long enough to enable thermal runaway (ignition) to occur. The total areal density (hot spot plus shell) is a crucial performance parameter in ICF and arguably the most difficult to control in today's ICF experiments.

The areal density of the imploded DT core directly enters into the Lawson criterion for ICF, which is typically written in terms of two measurable parameters: the areal density ρR and the neutron yield Y. As shown in Refs. [2–4], for ignition-relevant conditions, the Lawson triple product $nT\tau$ is approximately proportional to $\chi \sim (\rho R)_{2/3} Y_{1/3}$. To achieve conventional hot-spot ignition and gain at National Ignition Facility (NIF) energies [5,6], an areal density of about 1 g/cm^2 is a necessary requirement. Direct-drive implosions on OMEGA [7] and indirect-drive implosions on the NIF [8] are severely impacted by low areal densities below their design values [9–11].

Understanding and quantifying preheat due to energetic "hot" (~30- to 80-keV) electrons generated by laser–plasma instabilities has been a long-standing effort [12–22]. What is critically important is not the total amount of energy transferred to hot electrons, but the amount of energy that such electrons deposit inside the DT fuel, and more specifically, that portion of the DT fuel that produces the areal density confining the hot spot. As shown in this Letter for directly driven targets (with a DT layer enclosed by a thin plastic ablator), most hot electrons deposit their energy outside the relevant DT plasma, either in the plastic ablator or in the ablated DT plasma, both irrelevant to the core areal density. Therefore, measurements of the laser energy conversion into hot electrons do not provide a meaningful assessment of preheat because they include hot-electron energy that does not contribute to preheat of the dense unablated fuel. Experiments on electron divergence were useful for tuning hot-electron models with respect to electron directionality but they measure neither the energy deposited into the DT fuel nor its distribution within the fuel [23–26]. Different laser beam and plasma characteristics in addition to self-generated magnetic fields [27] in the coronal plasma and around the stalk mount [28] alter the transport and directionality of the hot electrons, making direct measurements of preheat energy deposition in DT all the more necessary.

In this Letter, we present the first direct measurements of hot-electron energy deposition within the DT fuel layer. This is accomplished using two implosions, one with both

DT and CH-ablator layers and one with a mass-equivalent CH-ablator-only shell. A new measurement based on the difference between the hard x-ray emission in the two implosions is developed to infer the preheat energy inside the entire DT layer. The spatial distribution of preheat energy within the DT is then inferred from a separate set of experiments using Cu-doped CH inner layers of varying thicknesses as proxies for different depths of DT fuel. The measured hot-electron energy deposition profile is then used to evaluate the areal-density degradation. The resulting areal density is shown to be in good agreement with the measured areal density in implosions with both moderate and high preheat levels. This technique can be used to measure spatial deposition of hot-electron energy in most laser fusion schemes and high-energy-density physics experiments.

In indirect- and direct-drive targets on the NIF, the primary instability generating hot electrons is stimulated Raman scattering (SRS) occurring in the underdense plasma below the quarter-critical density [29–31]. At the OMEGA scale, SRS is suppressed and the main instability is two-plasmon decay (TPD) [32,33]. Both SRS and TPD drive large-amplitude nonlinear electron plasma waves, which then transfer their energy to plasma electrons via Landau damping. It is for this reason that both instabilities have been an active part of theoretical [34–52] and experimental [53–80] research since the early days of the inertial fusion program. The presence of hot electrons in experiments is routinely measured on the NIF and OMEGA through the bremsstrahlung radiation they emit as they slow down in the plasma or hohlraum walls. On OMEGA, the hard x rays (HXRs) are primarily diagnosed from the four-channel hard x-ray detector (HXRD) [76]. The four channels are filtered to pass x rays above 20 keV, 40, 60, and 80 keV. The hot-electron temperature ($T_{\rm hot}$) is obtained through the (χ^2) minimization analysis described in Ref. [76] using a fit to a Maxwellian distribution. The conversion of the raw signal into mJ of radiated energy is described in Ref. [77] and assumes an isotropic emission of hard x rays.

To measure the energy deposited within the DT layer, it is necessary to determine what fraction of the hard x rays are emitted by electrons slowing down in DT. This is accomplished by imploding two targets (Fig. 1): the DT layered target with an outer plastic (CH or CD) ablator shell and an inner DT ice layer, and an ablator-only target with the same mass of the layered target. The two targets are imploded with the same pulse shape to produce the same hot-electron source since both targets exhibit the same plasma coronal conditions due to their hydrodynamic equivalency. This is illustrated in Fig. 1 which shows a simple schematic of the two different targets. The radiative efficiency (hard x-ray radiated energy per Joule of preheat energy deposited) primarily depends on the material's atomic number Z. The hard x rays measured in the two

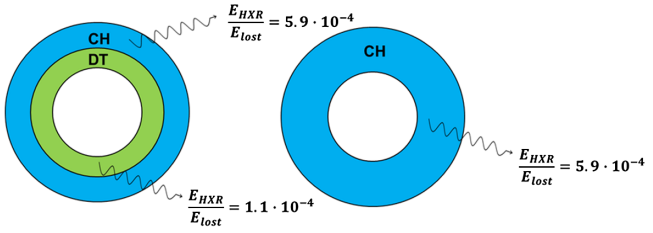

FIG. 1. Simple illustration of the hard x-ray comparison between an all-CH target and a DT-layered target. When the hot electron source is the same, the difference in hard x-ray signal is a direct indicator of electron deposition into the inner DT which emits less x rays for the same amount of preheat energy compared to CH.

implosions differ only because, in the DT layered target, some of the hot electrons slow down in DT rather than in plastic. The measurable difference in hard x-ray signals is shown in Fig. 2 which plots the measured hard x-ray signals for DT-layered shot 77 064 and its all-CH companion 77 062.

The difference in the hard x-ray signals is therefore proportional to the preheat energy deposited in the DT layer (payload):

$$E_{\rm payload}^{\rm preheat} = \frac{E_{\rm all\ CH}^{\rm HXR} - E_{\rm layered}^{\rm HXR}}{(E_{\rm HXR}/E_{\rm lost})_{\rm CH} - (E_{\rm HXR}/E_{\rm lost})_{\rm payload}}, \quad (1)$$

where $E_{\rm payload}^{\rm preheat}$ is the hot-electron energy deposited into the payload, $E_{\rm layered}^{\rm HXR}$ is the total energy radiated by hot electrons slowing down in the layered capsule with a payload, and $E_{\rm all\ CH}^{\rm HXR}$ is the total energy radiated by hot electrons in the all-CH target. The parameter $E_{\rm HXR}/E_{\rm lost}$ is the radiative efficiency for electrons slowing down in a given material. It represents the hard x rays emitted per unit energy deposited by hot electrons. For a given material, the parameter

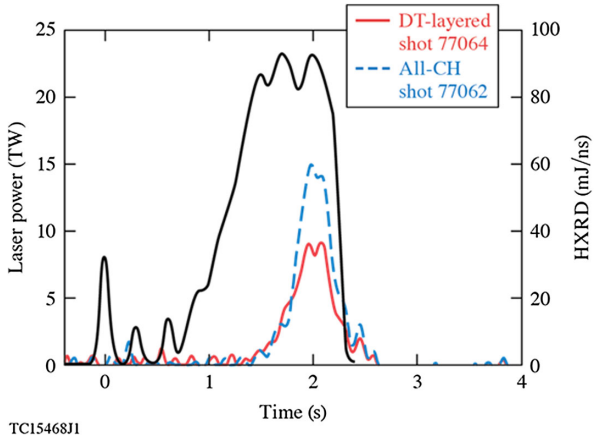

FIG. 2. The laser pulse (black) and the hard x-ray signals for DT-layered shot 77 064 (red) and all-CH shot 77 062 (blue) are plotted as a function of time. The difference in hard x-ray signals is proportional to the hot-electron energy deposited in the DT layer.

E_{HXR}/E_{lost} depends primarily on the atomic number ($\langle Z^2\rangle/\langle Z\rangle$) and the hot-electron temperature T_{hot} for a Maxwellian distribution. The radiative efficiency is calculated using NIST tables for the hard x-ray emission [81] and the stopping power from Ref. [82]. Note that in the derivation of the preheat formula, it is assumed that because the hot electron source is the same, the total preheat energy deposited into the all-CH target equals the sum of the preheat energy deposited into the payload plus the CH ablator for the layered implosion.

The formula in Eq. (1) is valid for any payload (DT or other material different from outer ablator) and irrespective of how the hot electrons are transported. This is shown in Fig. 3, which compares the preheat energy from Eq. (1) to the results of numerical simulations for different hot-electron sources and different payload materials using the radiation-hydrodynamic code LILAC [83]. Hot electrons are modeled by transferring a fraction of laser energy to electrons at the quarter-critical surface with a Maxwellian energy distribution, a prescribed hot-electron temperature T_{hot}, and a prescribed source divergence angle. Electron refluxing in the corona is accounted for by imposing an electrostatic sheath at the last boundary cell, which reflects electrons at random angles. This model is described in more detail in Ref. [84]. LILAC simulations used in Fig. 3 include

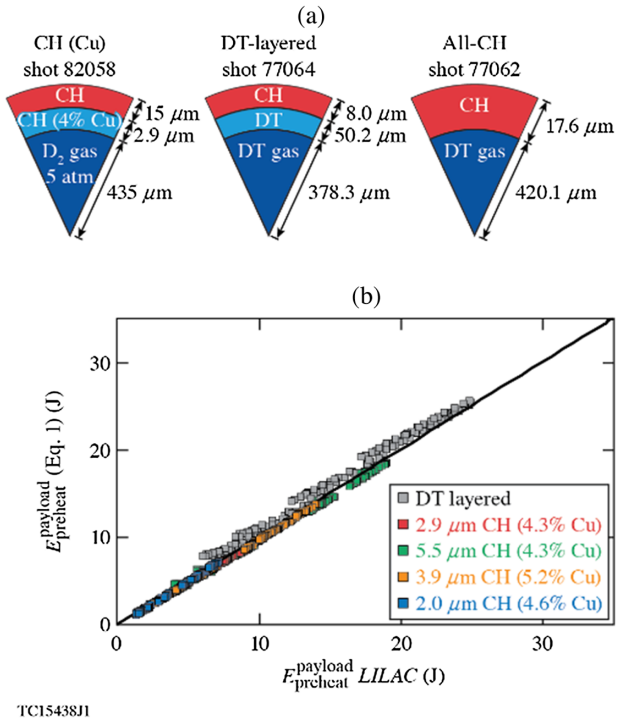

FIG. 3. (a) Typical targets used in preheat experiments and in the simulation ensemble. (b) The hot-electron energy deposited into a non-CH payload from Eq. (1) is compared to the results of LILAC simulations (bottom plot). Both the hot-electron source and the payload material are varied in the simulations. The good agreement validates the preheat formula [Eq. (1)].

layered shot 77 064 under varying preheat scenarios [85]. This implosion was driven on an adiabat of ~4 with ~26 kJ of laser energy and a peak intensity of $\sim 9 \times 10^{14}$ W/cm^2. In these simulations, the electrons are initialized at a temperature of 60 keV. Two variables are used to change the hot-electron energy deposition: (i) the total energy into fast electrons and (ii) divergence angle of the hot-electron source. Figure 3 also includes simulations where the DT payload is replaced with mass-equivalent layer of Cu-doped CH to demonstrate that the formula is independent of payload material. The good agreement shown in Fig. 3 indicates that the preheat formula Eq. (1) measures hot-electron energy deposition in the payload independently of hot-electron transport physics.

Although Eq. (1) directly measures the energy deposited into all of the DT, it is important to determine the spatial deposition profile within the DT. This was accomplished using warm targets replacing DT ice with a payload of Cu-doped plastic. This material was chosen for providing a higher HXR radiative efficiency than CH to enable measurement of the difference in HXR between all-CH and multilayer targets without major changes to the hydrodynamics. The thickness of the inner payload was varied to measure the spatial electron deposition within the unablated mass. The objective was to derive an energy deposition model that reproduces the measured hard x-ray signal from hot electrons in different payload layers. Payload thicknesses of 2, 2.9, 3.9, and 5.5 μm were used with Cu dopant fractions of $\sim 4.5 +/- 0.5\%$. This dopant fraction ensures that the hard x-ray signals will be large enough to create a measurable difference compared to the all-CH hard x-ray signal. The outer CH thickness of the layered targets was adjusted to keep the layered implosions mass equivalent to the all-CH target. This ensures the quarter-critical positions are approximately in the same locations for all implosions. As expected, LILAC simulations indicate that the parameters governing the TPD instability (quarter-critical temperature, intensity, and density scale length) are equal between the all-CH and the CH(Cu) implosions. Therefore, the difference in hard x-rays between all-CH targets and targets with CH(Cu) payload is proportional to the hot electrons slowing down in the CH(Cu) layer [Eq. (1)].

These experiments used the same pulse shape shown in Fig. 2. Another pulse with a slightly lower intensity of 7×10^{14} W/cm^2 was also used to study variations of the hot-electron source. The targets are shown in Fig. 3 and the pulse shape in Fig. 2. The total hot-electron energy E^{hot}_{tot} is determined from the hard x-ray measurement via the following formula:

$$E^{hot}_{tot} = \frac{E^{HXR}_{all\ CH}}{(E_{HXR}/E_{lost})_{CH}}. \quad (2)$$

It is found that $T_{hot} = 60 \pm 4$ keV and $E^{hot}_{tot} = 44 \pm 5$ J for the high-intensity implosions and $T_{hot} = 62 \pm 10$ keV and $E^{hot}_{tot} = 14 \pm 4$ J for the low-intensity implosions.

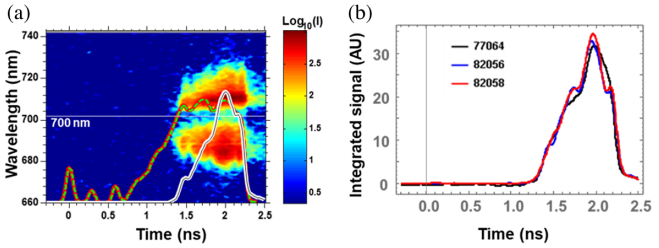

FIG. 4. (a) The half-harmonic spectrum for all-CH implosion 82 056. (b) The signal integrated over all frequencies is plotted as a function of time for DT-layered implosion 77 064, all-CH implosion 82056, and CH + CH(Cu) implosion 82058.

Before Eq. (1) is applied, it is important to verify that the hot-electron source is the same between all-CH and implosions with different payloads [either CH(Cu) or DT]. The assumption that the TPD activity does not vary from shot to shot was verified by comparing the scattered-light spectrum around half the original laser frequency. Emission near $1/2\omega$ is caused by many processes linked to the TPD instability and measured by calorimeters [86]. A comparison of the $1/2\omega$ signal between CH + CH(Cu), DT-layered and all-CH targets is shown in Fig. 4. The good agreement indicates there are no differences in TPD activity, thereby validating the primary assumption that the hot-electron source is the same between all hydro-equivalent targets. Details about the measurements of the half-omega signals and the cross calibrations applied in the comparisons are provided in the Supplemental Material [87].

In Fig. 5, the hard x-ray data for the different CH(Cu) implosions is plotted as a function of model predictions assuming uniform deposition of electrons within the payload. This implies that for a given hot-electron energy source $E_{\rm tot}$, de/dm is a constant K, where de is the preheat energy deposited into the mass dm,

$$K \equiv \frac{1}{E_{\rm tot}} \frac{de}{dm}. \tag{3}$$

It follows that the energy deposited into the payload is given by $KE_{\rm tot}M_p$, where M_p is the CH(Cu) payload mass. The value of K is varied to minimize χ^2 for the hard x-ray signals that are modeled as follows:

$$E^{\rm HXR}_{\rm CH(Cu)} = E_{\rm tot} K M_p \left(\frac{E_{\rm HXR}}{E_{\rm lost}}\right)_{\rm CH(Cu)} + E_{\rm tot}(1 - KM_{\rm p}) \left(\frac{E_{\rm HXR}}{E_{\rm lost}}\right)_{\rm CH}. \tag{4}$$

The above model is fit to eight different hard x-ray signals (four payload thicknesses for each pulse shape) and the χ^2 minimization leads to $K \approx 0.039 \pm 0.006\ \mu{\rm g}^{-1}$. The good agreement in Fig. 5 between the measurements and

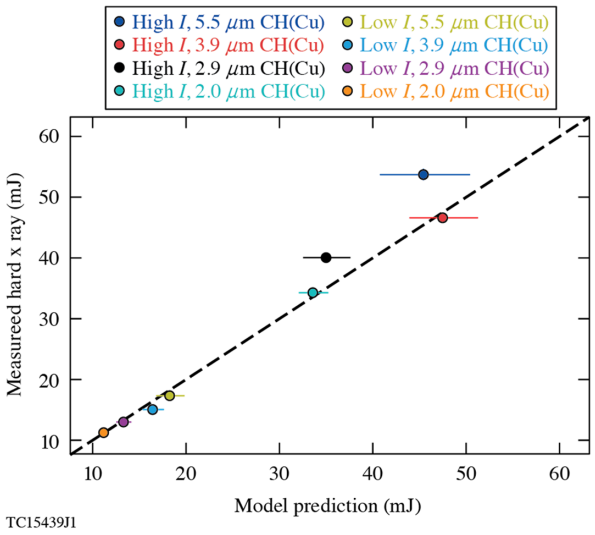

FIG. 5. The hard x-ray predictions from a uniform deposition model [Eq. (4)] are compared to the measured hard x-ray signals from the CH(Cu) experiments. The good agreement indicates the electrons deposit their energy uniformly in the unablated mass.

predictions from the uniform deposition model implies that for DT layered implosions, the preheat energy into the stagnated DT mass ($E^{\rm preheat}_{\rm stag}$) can be related to the total preheat energy into the entire DT via the mass ratio

$$E^{\rm preheat}_{\rm stag} \simeq \frac{M_{\rm stag}}{M_{\rm DT}} E^{\rm preheat}_{\rm DT}, \tag{5}$$

where $M_{\rm stag}$ is the stagnated DT mass, $M_{\rm DT}$ is the total DT mass and $E^{\rm preheat}_{\rm DT}$ is the total preheat energy in DT from Eq. (1).

The next step is to determine how the preheat energy relates to performance degradation. In Fig. 6, the

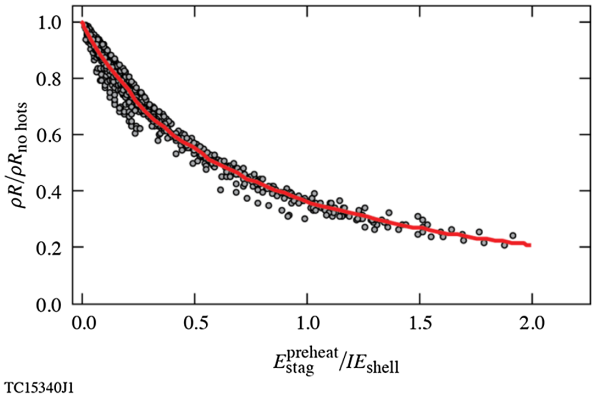

FIG. 6. Areal-density degradation versus preheat energy into the stagnated shell $E^{\rm preheat}_{\rm stag}$ normalized to the shell internal energy at peak velocity ${\rm IE}_{\rm shell}$ for a large ensemble of LILAC simulations with preheat energies ranging from 0 to 100 J and design adiabats between 2 and 5.5. The black curve is the best fit in Eq. (6).

TABLE I. Areal density (ρR) degradation for OMEGA DT-layered $\alpha \approx 4$ implosions.

Shot number	77 064	85 784	91 830	91 834
$E_{\text{hot}}^{\text{tot}}$ (J)	44.0 ± 5.0	43.8 ± 14.7	104.6 ± 35.0	104.6 ± 35.0
$E_{\text{DT}}^{\text{preheat}}$ (J)	13.0 ± 4.8	21.5 ± 7.1	48.1 ± 11.5	40.5 ± 13.7
$E_{\text{stag}}^{\text{preheat}}$ (J)	4.9 ± 2.1	7.5 ± 2.5	15.0 ± 4.7	11.6 ± 3.9
IE_{shell} (J)	43.0	43.1	48.1	48.0
ρR_{exp} (mg/cm^2)	201 ± 17	154 ± 13	120 ± 9	127 ± 11
$\rho R_{1\text{-}D}$ (mg/cm^2)	225	186	184	188
ρR_{hot} (mg/cm^2)	190 ± 16	156 ± 13	124 ± 15	135 ± 15

degradation in areal density is plotted as a function of the hot electron preheat energy normalized to the stagnated shell internal energy. The stagnated shell mass is defined as the mass enclosed by the rebound shock [3,88] at peak neutron rate. It was shown in Ref. [18] that the adiabat increase due to preheat can be written as

$$\alpha_{\text{hot}}/\alpha_{\text{no hot}} = (1 + E_{\text{stag}}^{\text{preheat}}/\text{IE}_{\text{shell}})^{3/5},$$

where $E_{\text{stag}}^{\text{preheat}}$ is the preheat energy into the stagnated shell and IE_{shell} is the shell internal energy at peak implosion velocity. Using the scaling $\rho R \sim \alpha^{-4/5}$, the ρR degradation can be written as

$$\frac{\rho R_{\text{hot}}}{(\rho R)_{\text{no hot}}} \approx \left(1 + 1.16\frac{E_{\text{stag}}^{\text{preheat}}}{\text{IE}_{\text{shell}}}\right)^{-4/3} \quad (6)$$

with the 1.16 factor resulting from the best fit to a LILAC simulation ensemble with a ~5% standard deviation.

The preheat energy and areal-density degradation for DT-layered implosions is determined using the preheat model consisting of the preheat energy measurement [Eqs. (1) and (5)] and the ρR degradation model [Eq. (6)]. Table I shows the preheat energies, ρR measurements [89,90], the LILAC-simulated ρR (ρR_{LILAC}), and the predicted ρR when preheat is included using Eq. (6) (ρR_{hot}) for different implosions with similar adiabats (of ~4). For moderate preheat (shots 77 064 and 85 784), ρR degradations of 10% to 20% are consistently observed and accurately predicted by the preheat model. For high preheat (shots 91 830, 91 834 [91]), the ρR degradation is larger (~40%) and also well predicted.

In summary, hot-electron preheat in the dense fuel of DT-layered direct-drive implosions was directly measured for the first time. Our results indicate a loss of areal density ranging from 10% to 40% for DT-layered implosions on OMEGA. This technique is currently being used to measure preheat in direct-drive implosions on the NIF—a critical factor for assessing the viability of the direct-drive path to ignition on megajoule-scale lasers [92].

This material is based upon work supported by the Department of Energy National Nuclear Security Administration under Award No. DE-NA0003856, the University of Rochester, and the New York State Energy Research and Development Authority. This report was prepared as an account of work sponsored by an agency of the U.S. Government. Neither the U.S. Government nor any agency thereof, nor any of their employees, makes any warranty, express or implied, or assumes any legal liability or responsibility for the accuracy, completeness, or usefulness of any information, apparatus, product, or process disclosed, or represents that its use would not infringe privately owned rights. Reference herein to any specific commercial product, process, or service by trade name, trademark, manufacturer, or otherwise does not necessarily constitute or imply its endorsement, recommendation, or favoring by the U.S. Government or any agency thereof. The views and opinions of authors expressed herein do not necessarily state or reflect those of the U.S. Government or any agency thereof.

[1] S. Atzeni and J. Meyer-ter-Vehn, The Physics of Inertial Fusion: Beam Plasma Interaction, Hydrodynamics, Hot Dense Matter, 1st ed., in *International Series of Monographs on Physics* Vol.125 (Oxford University Press, Oxford, 2004); J. D. Lindl, *Inertial Confinement Fusion: The Quest for Ignition and Energy Gain Using Indirect Drive* (Springer-Verlag, New York, 1998).

[2] R. Betti, A. R. Christopherson, B. K. Spears, R. Nora, A. Bose, J. Howard, K. M. Woo, M. J. Edwards, and J. Sanz, Phys. Rev. Lett. **114**, 255003 (2015).

[3] A. R. Christopherson, R. Betti, J. Howard, K. M. Woo, A. Bose, E. M. Campbell, and V. Gopalaswamy, Phys. Plasmas **25**, 072704 (2018).

[4] B. K. Spears, S. Glenzer, M. J. Edwards, S. Brandon, D. Clark, R. Town, C. Cerjan, R. Dylla-Spears, E. Mapoles, D. Munro *et al.*, Phys. Plasmas **19**, 056316 (2012).

[5] A. R. Christopherson, R. Betti, and J. D. Lindl, Phys. Rev. E **99**, 021201(R) (2019).

[6] J. D. Lindl, S. W. Haan, O. L. Landen, A. R. Christopherson, and R. Betti, Phys. Plasmas **25**, 122704 (2018).

[7] T. R. Boehly, D. L. Brown, R. S. Craxton, R. L. Keck, J. P. Knauer, J. H. Kelly, T. J. Kessler, S. A. Kumpan, S. J. Loucks, S. A. Letzring *et al.*, Opt. Commun. **133**, 495 (1997).

[8] E. M. Campbell and W. J. Hogan, Plasma Phys. Controlled Fusion **41**, B39 (1999).

[9] K. L. Baker, C. A. Thomas, D. T. Casey, S. Khan, B. K. Spears, R. Nora, T. Woods, J. L. Milovich, R. L. Berger, D. Strozzi *et al.*, Phys. Rev. Lett. **121**, 135001 (2018).

[10] S. Le Pape, L. F. Berzak Hopkins, L. Divol, A. Pak, E. L. Dewald, S. Bhandarkar, L. R. Bennedetti, T. Bunn, J. Biener, J. Crippen *et al.*, Phys. Rev. Lett. **120**, 245003 (2018).

[11] V. Gopalaswamy, R. Betti, J. P. Knauer, N. Luciani, D. Patel, K. M. Woo, A. Bose, I. V. Igumenshchev, E. M. Campbell, K. S. Anderson *et al.*, Nature (London) **565**, 581 (2019).

[12] W. L. Kruer, Phys. Fluids B **3**, 2356 (1991).

[13] E. M. Campbell, V. N. Goncharov, T. C. Sangster, S. P. Regan, P. B. Radha, R. Betti, J. F. Myatt, D. H. Froula, M. J. Rosenberg, I. V. Igumenshchev *et al.*, Matter Radiat. Extremes **2**, 37 (2017).

[14] R. S. Craxton, K. S. Anderson, T. R. Boehly, V. N. Goncharov, D. R. Harding, J. P. Knauer, R. L. McCrory, P. W. McKenty, D. D. Meyerhofer, J. F. Myatt *et al.*, Phys. Plasmas **22**, 110501 (2015).

[15] M. J. Rosenberg, A. A. Solodov, J. F. Myatt, W. Seka, P. Michel, M. Hohenberger, R. W. Short, R. Epstein, S. P. Regan, E. M. Campbell *et al.*, Phys. Rev. Lett. **120**, 055001 (2018).

[16] A. A. Solodov, M. J. Rosenberg, W. Seka, R. Epstein, J. F. Myatt, M. Hohenberger, R. Epstein, C. Stoeckl, R. W. Short, S. P. Regan *et al.*, Phys. Plasmas **27**, 052706 (2020).

[17] V. A. Smalyuk, D. Shvarts, R. Betti, J. A. Delettrez, D. H. Edgell, V. Yu. Glebov, V. N. Goncharov, R. L. McCrory, D. D. Meyerhofer, P. B. Radha *et al.*, Phys. Rev. Lett. **100**, 185005 (2008).

[18] D. Shvarts, V. A. Smalyuk, R. Betti, J. A. Delettrez, D. H. Edgell, V. Yu. Glebov, V. N. Goncharov, R. L. McCrory, P. W. McKenty, D. D. Meyerhofer *et al.*, J. Phys. Conf. Ser. **112**, 022005 (2008).

[19] T. Döppner, C. A. Thomas, L. Divol, E. L. Dewald, P. M. Celliers, D. K. Bradley, D. A. Callahan, S. N. Dixit, J. A. Harte, S. M. Glenn *et al.*, Phys. Rev. Lett. **108**, 135006 (2012).

[20] E. L. Dewald, F. Hartemann, P. Michel, J. Milovich, M. Hohenberger, A. Pak, O. L. Landen, L. Divol, H. F. Robey, O. A. Hurricane *et al.*, Phys. Rev. Lett. **116**, 075003 (2016).

[21] C. Stoeckl, R. E. Bahr, B. Yaakobi, W. Seka, S. P. Regan, R. S. Craxton, J. A. Delettrez, R. W. Short, J. Myatt, A. V. Maximov *et al.*, Phys. Rev. Lett. **90**, 235002 (2003).

[22] R. K. Follett, D. H. Edgell, R. J. Henchen, S. X. Hu, J. Katz, D. T. Michel, J. F. Myatt, J. Shaw, and D. H. Froula, Phys. Rev. E **91**, 031104(R) (2015).

[23] B. Yaakobi, C. Stoeckl, T. Boehly, D. D. Meyerhofer, and W. Seka, Phys. Plasmas **7**, 3714 (2000).

[24] B. Yaakobi, C. Stoeckl, W. Seka, J. A. Delettrez, T. C. Sangster, and D. D. Meyerhofer, Phys. Plasmas **12**, 062703 (2005).

[25] B. Yaakobi, A. A. Solodov, J. F. Myatt, J. A. Delettrez, C. Stoeckl, and D. H. Froula, Phys. Plasmas **20**, 092706 (2013).

[26] B. Yaakobi, P.-Y. Chang, A. A. Solodov, C. Stoeckl, D. H. Edgell, R. S. Craxton, S. X. Hu, J. F. Myatt, F. J. Marshall, W. Seka *et al.*, Phys. Plasmas **19**, 012704 (2012).

[27] J. R. Rygg, F. H. Séguin, C. K. Li, J. A. Frenje, M. J.-E. Manuel, R. D. Petrasso, R. Betti, J. A. Delettrez, O. V. Gotchev, J. P. Knauer *et al.*, Science **319**, 1223 (2008).

[28] N. Sinenian, M. J.-E. Manuel, J. A. Frenje, F. H. Seguin, C. K. Li, and R. D. Petrasso, Plasma Phys. Controlled Fusion **55**, 045001 (2013).

[29] W. L. Kruer, The Physics of Laser Plasma Interactions, in *Frontiers in Physics* Vol. 73, edited by D. Pines (Addison-Wesley, Redwood City, CA, 1988).

[30] C. S. Liu, M. N. Rosenbluth, and R. B. White, Phys. Rev. Lett. **31**, 697 (1973).

[31] M. N. Rosenbluth, Phys. Rev. Lett. **29**, 565 (1972).

[32] C. S. Liu and M. N. Rosenbluth, Phys. Fluids **19**, 967 (1976).

[33] A. Simon, R. W. Short, E. A. Williams, and T. Dewandre, Phys. Fluids **26**, 3107 (1983).

[34] D. E. Hinkel, M. D. Rosen, E. A. Williams, A. B. Langdon, C. H. Still, D. A. Callahan, J. D. Moody, P. A. Michel, R. P. J. Town, R. A. London *et al.*, Phys. Plasmas **18**, 056312 (2011).

[35] B. J. Winjum, J. E. Fahlen, F. S. Tsung, and W. B. Mori, Phys. Rev. Lett. **110**, 165001 (2013).

[36] W. Rozmus, R. P. Sharma, J. C. Samson, and W. Tighe, Phys. Fluids **30**, 2181 (1987).

[37] W. Rozmus, T. Chapman, A. Brantov, B. J. Winjum, R. L. Berger, S. Brunner, V. Yu. Bychenkov, A. Tableman, M. Tzoufras, and S. Glenzer, Phys. Plasmas **23**, 012707 (2016).

[38] T. Chapman, S. Hüller, P. E. Masson-Laborde, A. Heron, D. Pesme, and W. Rozmus, Phys. Rev. Lett. **108**, 145003 (2012).

[39] D. J. Strozzi, D. S. Bailey, P. Michel, L. Divol, S. M. Sepke, G. D. Kerbel, C. A. Thomas, J. E. Ralph, J. D. Moody, and M. B. Schneider, Phys. Rev. Lett. **118**, 025002 (2017).

[40] L. Yin, B. J. Albright, H. A. Rose, K. J. Bowers, B. Bergen, R. K. Kirkwood, D. E. Hinkel, A. B. Langdon, P. Michel, D. S. Montgomery *et al.*, Phys. Plasmas **19**, 056304 (2012).

[41] B. J. Albright, L. Yin, and B. Afeyan, Phys. Rev. Lett. **113**, 045002 (2014).

[42] J. Li, R. Yan, and C. Ren, Phys. Plasmas **24**, 052705 (2017).

[43] T. Kolber, W. Rozmus, and V. T. Tikhonchuk, Phys. Fluids B **5**, 138 (1993).

[44] J. Zhang, J. F. Myatt, R. W. Short, A. V. Maximov, H. X. Vu, D. F. DuBois, and D. A. Russell, Phys. Rev. Lett. **113**, 105001 (2014).

[45] J. F. Myatt, J. Zhang, J. A. Delettrez, A. V. Maximov, R. W. Short, W. Seka, D. H. Edgell, D. F. DuBois, D. A. Russell, and H. X. Vu, Phys. Plasmas **19**, 022707 (2012).

[46] J. F. Myatt, H. X. Vu, D. F. DuBois, D. A. Russell, J. Zhang, R. W. Short, and A. V. Maximov, Phys. Plasmas **20**, 052705 (2013).

[47] J. F. Myatt, J. Zhang, R. W. Short, A. V. Maximov, W. Seka, D. H. Froula, D. H. Edgell, D. T. Michel, I. V. Igumenshchev, D. E. Hinkel *et al.*, Phys. Plasmas **21**, 055501 (2014).

[48] R. Yan, A. V. Maximov, C. Ren, and F. S. Tsung, Phys. Rev. Lett. **103**, 175002 (2009).

[49] R. Yan, C. Ren, J. Li, A. V. Maximov, W. B. Mori, Z.-M. Sheng, and F. S. Tsung, Phys. Rev. Lett. **108**, 175002 (2012).

[50] R. K. Follett, J. F. Myatt, J. G. Shaw, D. T. Michel, A. A. Solodov, D. H. Edgell, B. Yaakobi, and D. H. Froula, Phys. Plasmas **24**, 102134 (2017).

[51] B. B. Afeyan and E. A. Williams, Phys. Plasmas **4**, 3827 (1997).

[52] R. K. Follett, J. G. Shaw, J. F. Myatt, J. P. Palastro, R. W. Short, and D. H. Froula, Phys. Rev. Lett. **120**, 135005 (2018).

[53] P. Michel, L. Divol, E. L. Dewald, J. L. Milovich, M. Hohenberger, O. S. Jones, L. Berzak Hopkins, R. L. Berger, W. L. Kruer, and J. D. Moody, Phys. Rev. Lett. **115**, 055003 (2015).

[54] M. J. Rosenberg, A. A. Solodov, W. Seka, R. K. Follett, J. F. Myatt, A. V. Maximov, C. Ren, S. Cao, P. Michel, M. Hohenberger *et al.*, Phys. Plasmas **27**, 042705 (2020).

[55] P. Michel, M. J. Rosenberg, W. Seka, A. A. Solodov, R. W. Short, T. Chapman, C. Goyon, N. Lemos, M. Hohenberger, J. D. Moody *et al.*, Phys. Rev. E **99**, 033203 (2019).

[56] B. J. MacGowan, B. B. Afeyan, C. A. Back, R. L. Berger, G. Bonnaud, M. Casanova, B. I. Cohen, D. E. Desenne, D. F. DuBois, A. G. Dulieu *et al.*, Phys. Plasmas **3**, 2029 (1996).

[57] R. K. Kirkwood, J. D. Moody, J. Kline, E. Dewald, S. Glenzer, L. Divol, P. Michel, D. Hinkel, R. Berger, E. Williams *et al.*, Plasma Phys. Controlled Fusion **55**, 103001 (2013).

[58] T. Gong, L. Hao, Z. Li, D. Yang, S. Li, X. Li, L. Guo, S. Zou, Y. Liu, X. Jiang *et al.*, Matter Radiat. Extremes **4**, 055202 (2019).

[59] R. P. Drake, E. A. Williams, P. E. Young, K. Estabrook, W. L. Kruer, H. A. Baldis, and T. W. Johnston, Phys. Rev. Lett. **60**, 1018 (1988).

[60] S. Depierreux, C. Neuville, C. Baccou, V. Tassin, M. Casanova, P.-E. Masson-Laborde, N. Borisenko, A. Orekhov, A. Colaitis, A. Debayle *et al.*, Phys. Rev. Lett. **117**, 235002 (2016).

[61] D. Turnbull, A. V. Maximov, D. H. Edgell, W. Seka, R. K. Follett, J. P. Palastro, D. Cao, V. N. Goncharov, C. Stoeckl, and D. H. Froula, Phys. Rev. Lett. **124**, 185001 (2020).

[62] D. T. Michel, A. V. Maximov, R. W. Short, J. A. Delettrez, D. Edgell, S. X. Hu, I. V. Igumenshchev, J. F. Myatt, A. A. Solodov, C. Stoeckl *et al.*, Phys. Plasmas **20**, 055703 (2013).

[63] D. H. Froula, D. T. Michel, I. V. Igumenshchev, S. X. Hu, B. Yaakobi, J. F. Myatt, D. H. Edgell, R. Follett, V. Yu. Glebov, V. N. Goncharov *et al.*, Plasma Phys. Controlled Fusion **54**, 124016 (2012).

[64] W. Seka, J. F. Myatt, R. W. Short, D. H. Froula, J. Katz, V. N. Goncharov, and I. V. Igumenshchev, Phys. Rev. Lett. **112**, 145001 (2014).

[65] W. Seka, D. H. Edgell, J. F. Myatt, A. V. Maximov, R. W. Short, V. N. Goncharov, and H. A. Baldis, Phys. Plasmas **16**, 052701 (2009).

[66] E. Fabre, F. Amiranoff, R. Fabbro, C. Garban-Labaune, J. Virmont, M. Weinfeld, F. David, and R. Pellat, in *Plasma Physics and Controlled Nuclear Fusion Research 1980* (IAEA, Vienna, 1981), Vol. 2, p. 263.

[67] C. Labaune, H. A. Baldis, E. Fabre, F. Briand, D. M. Villeneuve, and K. Estabrook, Phys. Fluids B **2**, 166 (1990).

[68] C. Rousseaux, F. Amiranoff, C. Labaune, and G. Matthieussent, Phys. Fluids B **4**, 2589 (1992).

[69] S. Depierreux, C. Neuville, C. Baccou, V. Tassin, M. Casanova, P.-E. Masson-Laborde, N. Borisenko, A. Orekhov, A. Colaitis, A. Debayle *et al.*, Phys. Rev. Lett. **117**, 235002 (2016).

[70] V. T. Tikhonchuk, Nucl. Fusion **59**, 032001 (2019).

[71] E. L. Dewald, L. J. Suter, C. Thomas, S. Hunter, D. Meeker, N. Meezan, S. H. Glenzer, E. Bond, J. Kline, S. Dixit *et al.*, J. Phys. Conf. Ser. **244**, 022074 (2010).

[72] E. L. Dewald, C. Thomas, S. Hunter, L. Divol, N. Meezan, S. H. Glenzer, L. J. Suter, E. Bond, J. L. Kline, J. Celeste *et al.*, Rev. Sci. Instrum. **81**, 10D938 (2010).

[73] J. W. McDonald, L. J. Suter, O. L. Landen, J. M. Foster, J. R. Celeste, J. P. Holder, E. L. Dewald, M. B. Schneider, D. E. Hinkel, R. L. Kauffman *et al.*, Phys. Plasmas **13**, 032703 (2006).

[74] T. Doppner, B. Bachmann, F. Albert, P. Bell, S. Burns, J. Celeste, R. Chow, L. Divol, E. L. Dewald, M. Hohenberger *et al.*, J. Instrum. **11**, P06010 (2016).

[75] M. Hohenberger, F. Albert, N. E. Palmer, J. J. Lee, T. Döppner, L. Divol, E. L. Dewald, B. Bachmann, A. G. MacPhee, G. LaCaille *et al.*, Rev. Sci. Instrum. **85**, 11D501 (2014).

[76] C. Stoeckl, V. Yu. Glebov, D. D. Meyerhofer, W. Seka, B. Yaakobi, R. P. J. Town, and J. D. Zuegel, Rev. Sci. Instrum. **72**, 1197 (2001).

[77] C. Stoeckl, W. Theobald, S. P. Regan, and M. H. Romanofsky, Rev. Sci. Instrum. **87**, 11E323 (2016).

[78] A. A. Solodov, B. Yaakobi, D. H. Edgell, R. K. Follett, J. F. Myatt, C. Sorce, and D. H. Froula, Phys. Plasmas **23**, 102707 (2016).

[79] M. Stoeckl and A. A. Solodov, Rev. Sci. Instrum. **89**, 063101 (2018).

[80] J. Trela, M Theobald, K. S. Anderson, D. Batani, R. Betti, A. Casner, J. A. Delettrez, J. A. Frenje, V. Yu. Glebov, X. Ribeyre *et al.*, Phys. Plasmas **25**, 052707 (2018).

[81] S. M. Seltzer and M. J. Berger, Nucl. Instrum. Methods Phys. Res., Sect. B **12**, 95 (1985).

[82] A. A. Solodov and R. Betti, Phys. Plasmas **15**, 042707 (2008).

[83] J. Delettrez, R. Epstein, M. C. Richardson, P. A. Jaanimagi, and B. L. Henke, Phys. Rev. A **36**, 3926 (1987).

[84] J. A. Delettrez, T. J. B. Collins, and C. Ye, Phys. Plasmas **26**, 062705 (2019).

[85] S. P. Regan, V. N. Goncharov, I. V. Igumenshchev, T. C. Sangster, R. Betti, A. Bose, T. R. Boehly, M. J. Bonino, E. M. Campbell, D. Cao *et al.*, Phys. Rev. Lett. **117**, 025001 (2016).

[86] W. Seka, D. H. Edgell, J. P. Knauer, J. F. Myatt, A. V. Maximov, R. W. Short, T. C. Sangster, C. Stoeckl, R. E. Bahr, R. S. Craxton *et al.*, Phys. Plasmas **15**, 056312 (2008).

[87] See Supplemental Material at http://link.aps.org/supplemental/10.1103/PhysRevLett.127.055001 for the supplement provides details about how the hard x-ray signal is converted into hot electron energy, how the radiative efficiencies are calculated, and provides justifications for the assumptions used in the preheat formula.

[88] R. Betti, P. Y. Chang, B. K. Spears, K. S. Anderson, J. Edwards, M. Fatenejad, J. D. Lindl, R. L. McCrory,

R. Nora, and D. Shvarts, Phys. Plasmas **17**, 058102 (2010).

[89] M. Gatu Johnson, J. A. Frenje, D. T. Casey, C. K. Li, F. H. Seguin, R. Petrasso, R. Ashabranner, R. M. Bionta, D. L. Bleuel, E. J. Bond *et al.*, Rev. Sci. Instrum. **83**, 10D308 (2012).

[90] C. J. Forrest, P. B. Radha, V. Yu. Glebov, V. N. Goncharov, J. P. Knauer, A. Pruyne, M. Romanofsky, T. C. Sangster, M. J. Shoup III, C. Stoeckl *et al.*, Rev. Sci. Instrum. **83**, 10D919 (2012).

[91] D. Cao, D. Patel, W. Theobald, M. J. Rosenberg, A. R. Christopherson, C. Stoeckl, I. V. Igumenshchev, V. Gopalaswamy, S. P. Regan, C. Thomas *et al.*, Measuring correlation between hot-electron preheat to shell ρR for layered, direct-drive inertial confinement fusion implosions on OMEGA (to be published).

[92] A. A. Solodov, M. J. Rosenberg, A. R. Christopherson, R. Betti, M. Stoeckl, W. Seka, R. Epstein, R. K. Follett, P. B. Radha, S. P. Regan *et al.*, Bull. Am. Phys. Soc. **64**, 00011 (2019).